Elasticity of lower-mantle bridgmanite

ARISING FROM A. Kurnosov, H. Marquardt, D. Frost, T. Boffa Ballaran & L. Ziberna *Nature* **543**, 543–546 (2017); https://doi.org/10.1038/nature21390

Bridgmanite ((Mg,Fe)(Fe,Al,Si)O_3) is believed to be the most abundant mineral in Earth's lower mantle, accounting for approximately 75% of the region by volume[1,2]. Recently, Kurnosov et al.[3] reported on the single-crystal elasticity of (Al,Fe)-bearing bridgmanite up to 40 GPa and concluded that a Fe^{3+}/Fe^{2+} ratio of about two is required to match Preliminary Reference Earth Model (PREM) seismic profiles[4] at depths below 1,200 km. Here we use a sensitivity test between measured velocities and elastic constants (C_{ij}) and a covariance matrix analysis to show that their derived elastic constants and velocities have large uncertainties at lower-mantle pressures. These uncertainties invalidate the assertion of ref. [3] of the existence of an Fe^{3+}-rich pyrolitic lower mantle with (Al,Fe)-bearing bridgmanite, and therefore further experimental studies at relevant lower-mantle pressure–temperature conditions are required to reliably infer the mineralogical and geochemical properties of the deep mantle. There is a Reply to this Comment by Kurnosov, A. et al. *Nature* **564**, https://doi.org/10.1038/s41586-018-0742-6 (2018).

Bridgmanite contains approximately 10% iron (in Fe^{2+} and Fe^{3+} states) and 5%–7% Al_2O_3 in its structure. Knowledge of the elasticity of (Al,Fe)-bearing bridgmanite at relevant pressure–temperature conditions is thus essential for comparison with the seismic models used to improve our understanding of the physics and chemistry of the lower mantle. In recent decades, there have been extensive experimental and theoretical efforts to obtain single-crystal elastic constants and polycrystalline aggregate compressional and shear-wave velocities (V_P and V_S) for (Al,Fe)-bearing bridgmanite at high-pressure and high-temperature conditions[5–11].

Bridgmanite crystallizes in an orthorhombic crystal structure at lower-mantle pressure–temperature conditions and exhibits nine independent C_{ij}. The longitudinal moduli (C_{11}, C_{22} and C_{33}) strongly correlate with the aggregate V_P value, whereas the shear moduli (C_{44}, C_{55} and C_{66}) determine the aggregate V_S value (Fig. 1, Supplementary Information). Reliable derivation of the nine C_{ij} in bridgmanite requires extensive experimental measurements of both V_P and V_S for crystallographic orientations that are intrinsically sensitive to longitudinal, shear and off-diagonal C_{ij} (Fig. 1a, b; Extended Data Fig. 1). Kurnosov et al.[3] used Brillouin scattering to measure the V_P and V_S values of single-crystal (Al,Fe)-bearing bridgmanite ($(Mg_{0.9}Fe_{0.1}Si_{0.9}Al_{0.1})O_3$) and X-ray diffraction to determine the crystallographic orientations and densities of two platelets in a high-pressure diamond anvil cell up to approximately 40 GPa. Analysis of the sensitivity of the crystal orientations between each C_{ij}, the direction-dependent velocities (V_P, V_{S1} and V_{S2}), and the number of measured phonon directions show that the crystal orientations in ref. [3] are appropriate for tightly constraining only some of the shear moduli[12]: C_{44} and C_{55} can be determined with

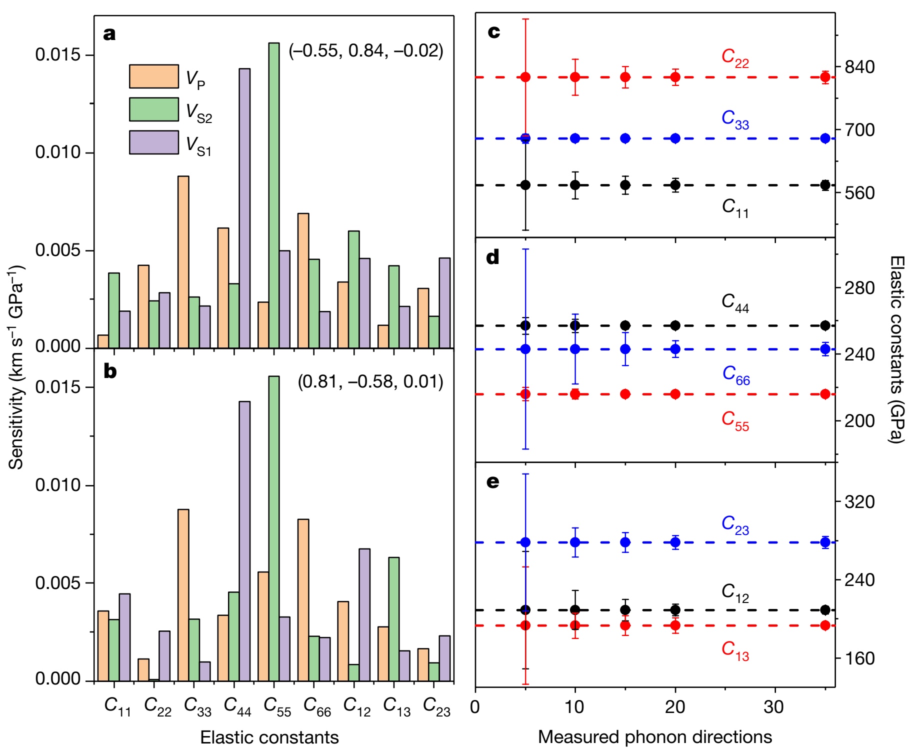

Fig. 1 | C_{ij} sensitivity to the velocities and number of measured phonon directions of single-crystal bridgmanite in two crystallographic orientations used in ref. [3] at 40.17 GPa. a, b, The sensitivity of V_P and two orthogonally polarized shear-wave velocities V_{S1} and V_{S2} in two orientations. The orientations of the two crystal platelets are given in parentheses. **c–e**, The sensitivity is used to evaluate the uncertainties of the elastic constants as a function of the number of measured phonon directions with 10° azimuthal separation (see Supplementary Information for details). Error bars represent standard deviations (1σ) of the elastic moduli.

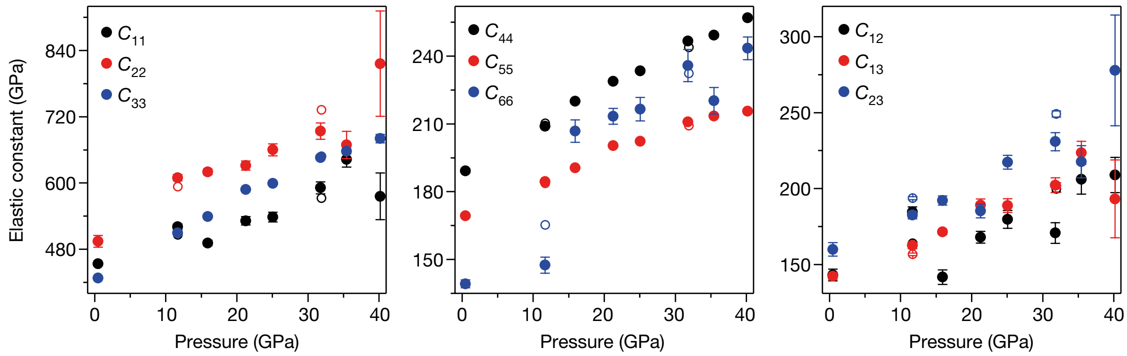

Fig. 2 | Derived full elastic constants of (Al,Fe)-bearing bridgmanite at high pressure. Filled data points are our calculated results using the raw velocity data in ref. [3] and the covariance matrix analysis; open data points are updated results in the Author Correction to ref. [3] using the global fit method (only two pressure points were provided in the first draft of their Reply). Error bars represent standard deviations (1σ) and are not shown when smaller than the symbols.

high sensitivity, but the orientations examined provide only weak constraints on longitudinal and off-diagonal moduli (Fig. 1c–e). We note that measuring the V_P of bridgmanite using Brillouin spectroscopy at high pressures in a diamond anvil cell is technically difficult because the sample's V_P is mostly blocked by the diamond V_S peak at pressures above approximately 23 GPa—the starting pressure at the top of the lower mantle. At 40.17 GPa, Kurnosov et al.[3] measured 15 phonon directions in V_P and 30 phonon directions in V_S. Based on our modelling, the uncertainties of the longitudinal and shear moduli at 40.17 GPa are approximately 2% and 0.5%–1%, respectively (Fig. 1c, d).

Christoffel's equation exactly defines the relationship between C_{ij}, the direction-dependent velocities, and the density of bridgmanite, and has been used to derive C_{ij} from velocity data. Finite-strain equations can also be applied to model high-pressure results to investigate the effects of pressure on elasticity. However, because there are nine C_{ij} variables involved in the analysis, the covariance matrix method is necessary to rigorously evaluate the uncertainties and correlations of the derived C_{ij} (Fig. 2)[13]. Our analysis of the data from ref. [3] using this method clearly shows that most C_{ij} above 25 GPa exhibit strong trade-offs of modelled values and their uncertainties among one another, with increased uncertainties at higher pressures (Supplementary Tables 2–9). In light of this, we consider the errors reported for C_{ij} in Kurnosov et al.[3] to be unrealistically low (Fig. 2). Kurnosov et al.[3] used a 'global fit' method to simultaneously account for all measured direction-dependent acoustic-wave velocities and densities at all experimental pressures. However, analysis of the global fit method and the derived C_{ij} by Kurnosov et al.[3] shows that the errors of C_{ij} at higher pressures above 25 GPa (with limited V_P data) are drastically reduced by lower-pressure data that have more V_P and V_S measurements with smaller errors. Since Christoffel's equation exactly defines the relationship between C_{ij} and the direction-dependent velocities, the greater errors in C_{ij} at higher pressures cannot be simply reduced and compensated by results obtained at lower pressures, even when the finite-strain equations are used concurrently in the modelling. Furthermore, analysis of the reported C_{ij} values and experimental velocity data in Kurnosov et al.[3] using Christoffel's equation at two representative pressures of 11.66 GPa and 31.76 GPa shows that their velocity data are inconsistent with the reported C_{ij}: the velocity fitting curve cannot be reproduced using their reported C_{ij} values, densities and crystallographic orientations (Extended Data Figs. 2 and 3).

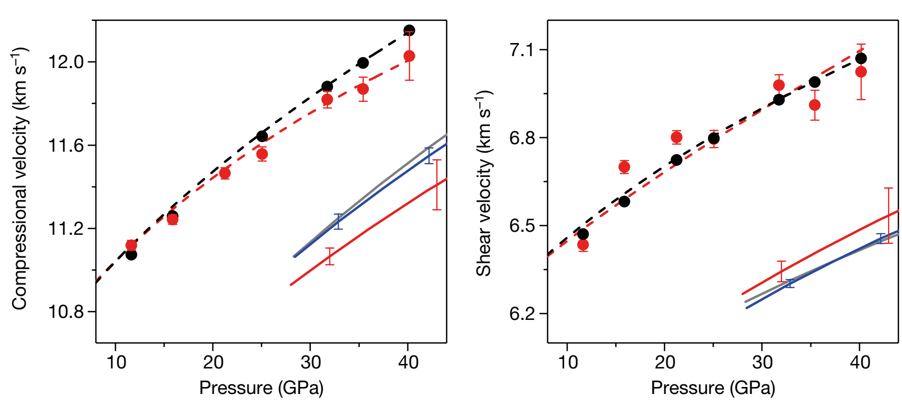

Fig. 3 | V_P and V_S profiles of the (Al,Fe)-bearing bridgmanite $(Mg_{0.9}Fe_{0.1}Si_{0.9}Al_{0.1})O_3$ in the lower mantle. V_P and V_S profiles in PREM[4] are also plotted for comparison (grey lines). Red filled circles are our calculated V_P and V_S values of the bridgmanite at high pressures and 300 K using our obtained adiabatic bulk modulus (K_S) and shear modulus (G); the red dashed lines are the finite-strain equation fits to our calculated data; the black filled circles are the V_P and V_S values of the bridgmanite at high pressures and 300 K reported in figure 2 of ref. [3]; and the black dashed lines are the finite-strain equation fits to their results. The solid red lines are our newly calculated aggregate V_P and V_S values for a simplified pyrolite model containing 80 vol% bridgmanite $((Mg_{0.9}Fe_{0.1}Si_{0.9}Al_{0.1})O_3)$ and 20 vol% ferropericlase $((Mg_{0.8}Fe_{0.2})O)$ along a representative geotherm using thermoelastic parameters reported by refs. [3] and [15]. The solid blue lines represent V_P and V_S values of a pyrolitic mantle along a representative geotherm reported by ref. [3]. Error bars represent standard deviations (1σ). The standard deviations of the red lines are estimated from our results using the sensitivity and covariance matrix analysis with standard error propagation, while the uncertainties of the blue lines are from ref. [3]. We note that our calculated V_P and V_S along a representative geotherm exhibit large uncertainties and could not be used to reliably constrain the lower-mantle composition.

Using the derived C_{ij}, the aggregate V_P and V_S of the bridgmanite can be calculated at high pressure and 300 K (Fig. 3; Extended Data Figs. 4–6). (Al,Fe)-bearing bridgmanite is only stable above approximately 23 GPa, and our analysis shows the uncertainties of both V_P and V_S to be about 0.5% at this pressure. At the highest pressure reported by ref. [3] (40.17 GPa), they report uncertainties in V_P and V_S of approximately 1.5% and 1.0%, respectively. The lower mantle is probably made up of 75% (Al,Fe)-bearing bridgmanite, 20% ferropericlase (approximately $(Mg_{0.8}Fe_{0.2})O$), and 5% calcium perovskite. Previous studies have also found that bridgmanite contains a significant amount of Fe^{3+} and that the partition coefficient of iron between bridgmanite and ferropericlase varies with increasing depth[1]. To make the modelling more difficult, a small amount of metallic iron could be formed in the lower mantle because of the charge disproportionation reaction in bridgmanite[14]. Elastic parameters and their uncertainties for these mineral phases as well as element partitioning need to be considered at lower-mantle pressure–temperature conditions to realistically investigate the geophysical consequences of the contributions of these components to seismic profiles. Our analysis shows that the uncertainties of V_P and V_S of bridgmanite at 40 GPa along an expected geotherm (or around 1,000 km in depth) are approximately 2.0% and 1%, respectively. Although Kurnosov et al.[3] stated that the V_P and V_S profiles of a pyrolitic mineralogical model are consistent with PREM[4], their uncertainties are of the order of a few per cent when taking the aforementioned contributions into account. These uncertainties are larger than the magnitude of the metallic iron and Fe^{3+} content effects (less than 0.5% according to figure 4a in ref. [3]) on the modelled lower-mantle V_P and V_S profiles. In fact, with such large uncertainties, the pyrolitic compositional model of the lower mantle can be called into question. Kurnosov et al.[3] also implied the presence of metallic iron, a change in bridgmanite Al-Fe cation ordering, or a decrease in the ferric iron content in the lower parts of the lower mantle. However, at the current resolution of the elastic constant results of lower-mantle minerals, the existence of metallic iron and Fe^{3+}-rich bridgmanite would be seismically invisible.

In summary, we consider the use of a sensitivity test and covariance matrix to be a rigorous approach for the investigation of the elastic constants of single-crystal bridgmanite and its aggregate sound velocities at high pressure. At present, the uncertainties of the V_P and V_S profiles of (Al,Fe)-bearing bridgmanite at relevant lower-mantle conditions are too large to support the existence of Fe^{3+}-rich bridgmanite and a small amount of metallic iron in the lower mantle. Accordingly, further experimental studies to gather extensive velocity data of C_{ij}-sensitive orientations at relevant lower-mantle pressure–temperature conditions should be performed on candidate phases such as bridgmanite and ferropericlase to reliably infer the mineralogical and geochemical properties of the deep mantle.

Data availability

The data that support the findings of this study are available from the corresponding author upon reasonable request.

Jung-Fu Lin[1]*, Zhu Mao[2], Jing Yang[1,3] & Suyu Fu[1]

[1]Department of Geological Sciences, Jackson School of Geosciences, The University of Texas at Austin, Austin, TX, USA. [2]Laboratory of Seismology and Physics of Earth's Interior, School of Earth and Planetary Sciences, University of Science and Technology of China, Hefei, China. [3]Geophysical Laboratory, Carnegie Institution for Science, Washington, DC, USA.
*e-mail: afu@jsg.utexas.edu

Received: 7 February 2018; Accepted: 13 September 2018
Published online 19 December 2018.

1. Irifune, T. et al. Iron partitioning and density changes of pyrolite in Earth's lower mantle. *Science* **327**, 193–195 (2010).
2. Lin, J. F., Speziale, S., Mao, Z. & Marquardt, H. Effects of the electronic spin transitions of iron in lower mantle minerals: implications for deep mantle geophysics and geochemistry. *Rev. Geophys*. **51**, 244–275 (2013).
3. Kurnosov, A., Marquardt, H., Frost, D., Boffa Ballaran, T. & Ziberna, L. Evidence for a Fe^{3+}-rich pyrolitic lower mantle from (Al,Fe)-bearing bridgmanite elasticity data. *Nature* **543**, 543–546 (2017); Author Correction *Nature* **558**, E3 (2018).
4. Dziewonski, A. M. & Anderson, D. L. Preliminary Reference Earth Model. *Phys. Earth Planet. Inter*. **25**, 297–356 (1981).
5. Li, B. S. & Zhang, J. Z. Pressure and temperature dependence of elastic wave velocity of $MgSiO_3$ perovskite and the composition of the lower mantle. *Phys. Earth Planet. Inter*. **151**, 143–154 (2005).
6. Wentzcovitch, R., Karki, B., Cococcioni, M. & De Gironcoli, S. Thermoelastic properties of $MgSiO_3$-perovskite: insights on the nature of the Earth's lower mantle. *Phys. Rev. Lett.* **92**, 018501 (2004).
7. Sinogeikin, S. V., Zhang, J. & Bass, J. D. Elasticity of single crystal and polycrystalline $MgSiO_3$ perovskite by Brillouin spectroscopy. *Geophys. Res. Lett.* **31**, L06620 (2004).
8. Murakami, M., Sinogeikin, S. V., Hellwig, H., Bass, J. D. & Li, J. Sound velocity of $MgSiO_3$ perovskite to Mbar pressure. *Earth Planet. Sci. Lett.* **256**, 47–54 (2007).
9. Murakami, M., Ohishi, Y., Hirao, N. & Hirose, K. A perovskitic lower mantle inferred from high-pressure, high-temperature sound velocity data. *Nature* **485**, 90–94 (2012).
10. Jackson, J. M., Zhang, J., Shu, J., Sinogeikin, S. V. & Bass, J. D. High-pressure sound velocities and elasticity of aluminous $MgSiO_3$ perovskite to 45 GPa: implications for lateral heterogeneity in Earth's lower mantle. *Geophys. Res. Lett.* **32**, L21305 (2005).
11. Fu, S. et al. Abnormal elasticity of Fe-bearing bridgmanite in the Earth's lower mantle. *Geophys. Res. Lett.* **45**, 4725–4732 (2018).
12. Yoneda, A. et al. Elastic anisotropy of experimental analogues of perovskite and post-perovskite help to interpret D″ diversity. *Nat. Commun.* **5**, 3453 (2014).
13. Abramson, E., Brown, J., Slutsky, L. & Zaug, J. The elastic constants of San Carlos olivine to 17 GPa. *J. Geophys. Res. Solid Earth* **102**, 12253–12263 (1997).
14. Frost, D. J. et al. Experimental evidence for the existence of iron-rich metal in the Earth's lower mantle. *Nature* **428**, 409–412 (2004).
15. Stixrude, L. & Lithgow-Bertelloni, C. Thermodynamics of mantle minerals—I. Physical properties. *Geophys. J. Int.* **162**, 610–632 (2005).

Author contributions J.-F.L. initiated the project. Z.M. performed the data processing using the covariance matrix. J.Y. and S.F. performed the sensitivity test analysis. Z.M. and S.F. performed elasticity modelling and error analysis. S.F. prepared the draft Supplementary Information. J.-F.L. wrote the manuscript and all authors participated in the manuscript revision.

Competing interests Declared none.

Additional information
Extended data accompanies this Comment.
Supplementary information accompanies this Comment.
Reprints and permissions information is available at http://www.nature.com/reprints.
Correspondence and requests for materials should be addressed to J.-F.L.

https://doi.org/10.1038/s41586-018-0741-7

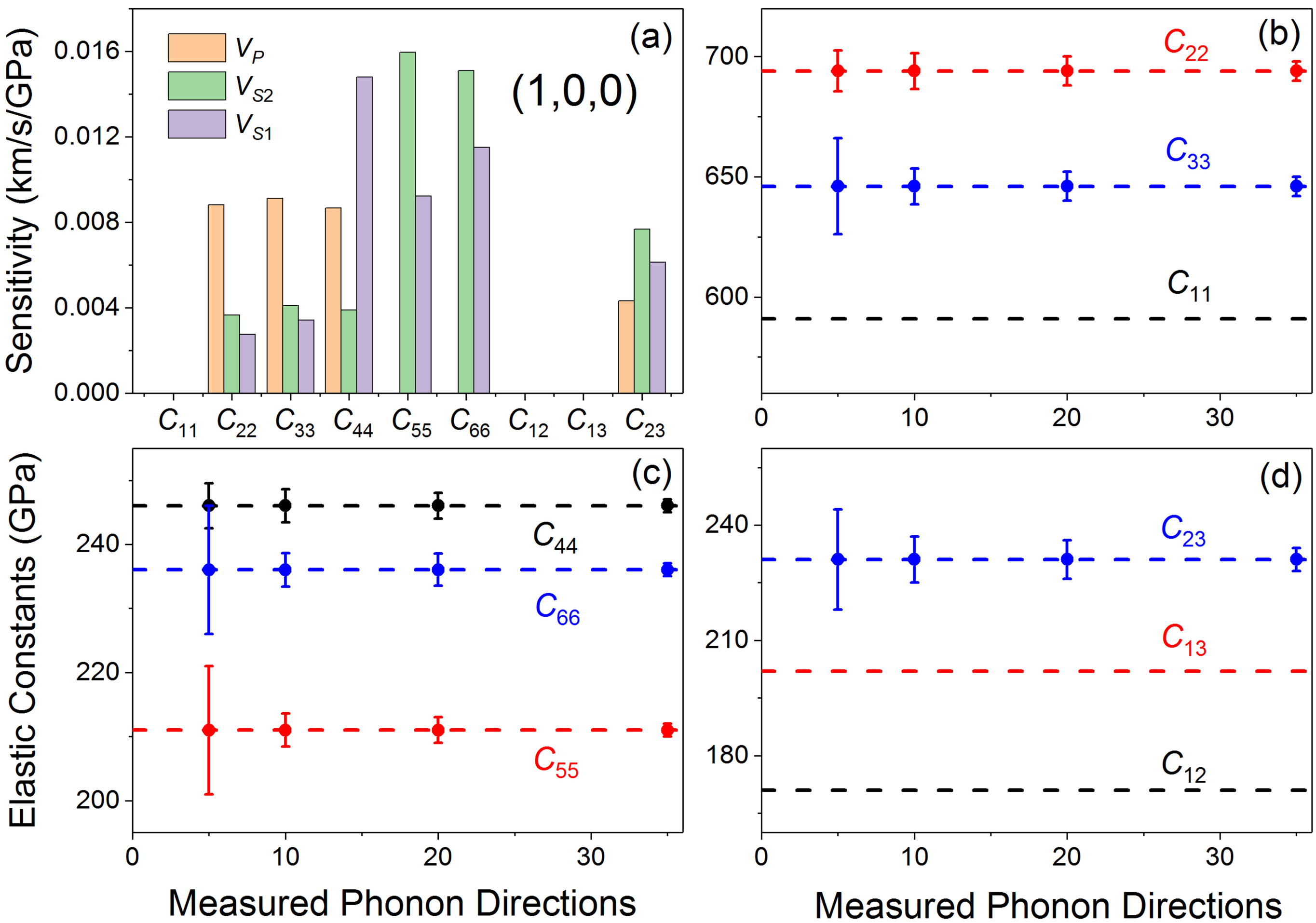

Extended Data Fig. 1 | Relationship between the uncertainties of the reported elastic constants and our calculated sensitivity of wave velocities for a chosen crystallographic (100) orientation as well as the number of measured phonon directions. a–d, The azimuthal angle between two adjacent phonon directions is 10°. Error bars in **b–d** represent standard deviations (1σ) of the elastic constants. Data on the elastic constants are from ref. [6].

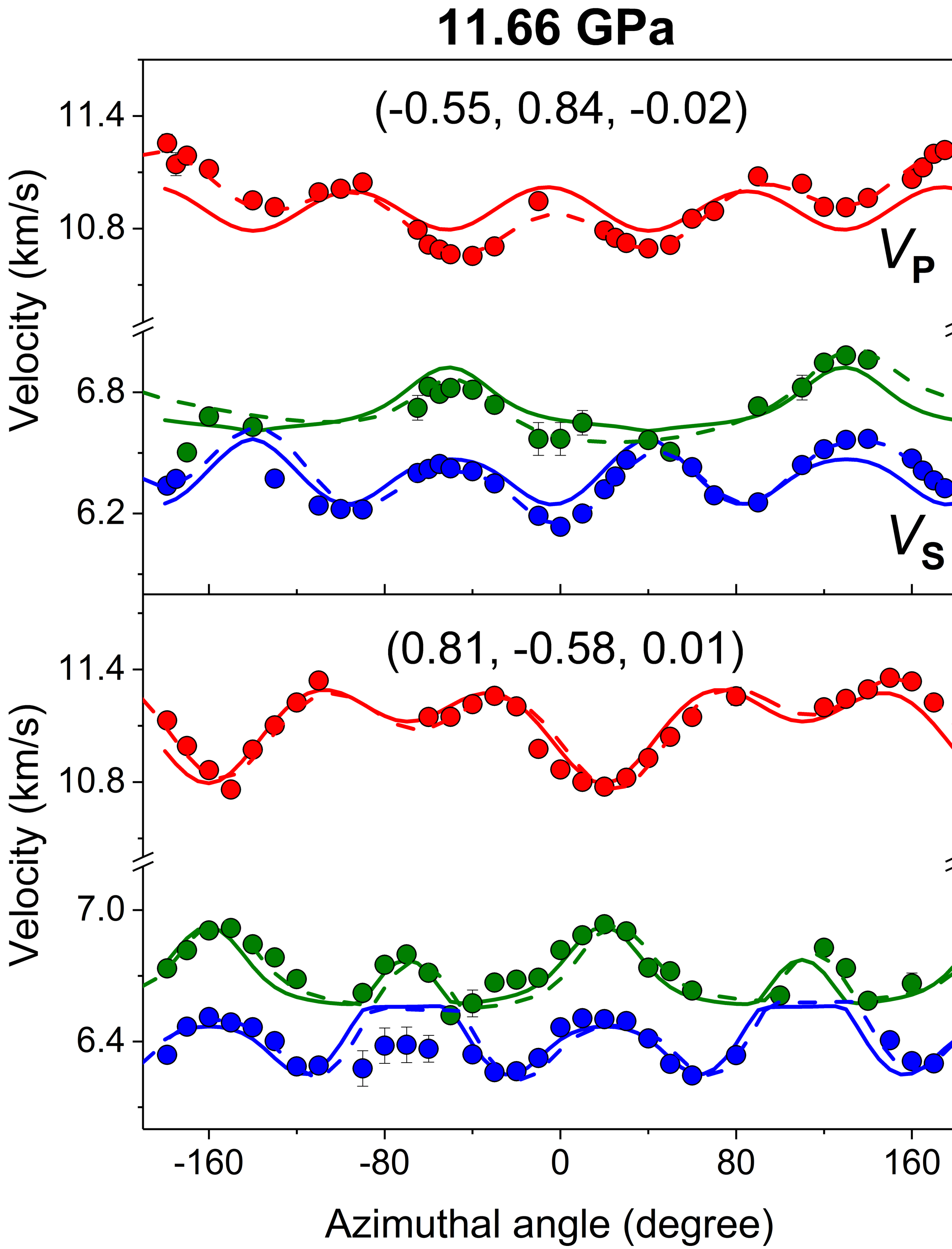

Extended Data Fig. 2 | Modelling the acoustic velocity of bridgmanite to derive C_{ij} at 11.66 GPa. Error bars are not shown when smaller than the symbols. Filled data points are the velocity data from Kurnosov et al.[3]; the dashed lines are velocity-fitting curves from Kurnosov et al.[3]; and the solid lines are velocity-fitting curves using the C_{ij} derived from the covariance matrix analysis in this study. Red, V_P; green, V_{S1}; blue, V_{S2}. The orientations of the crystal platelets are given in parentheses.

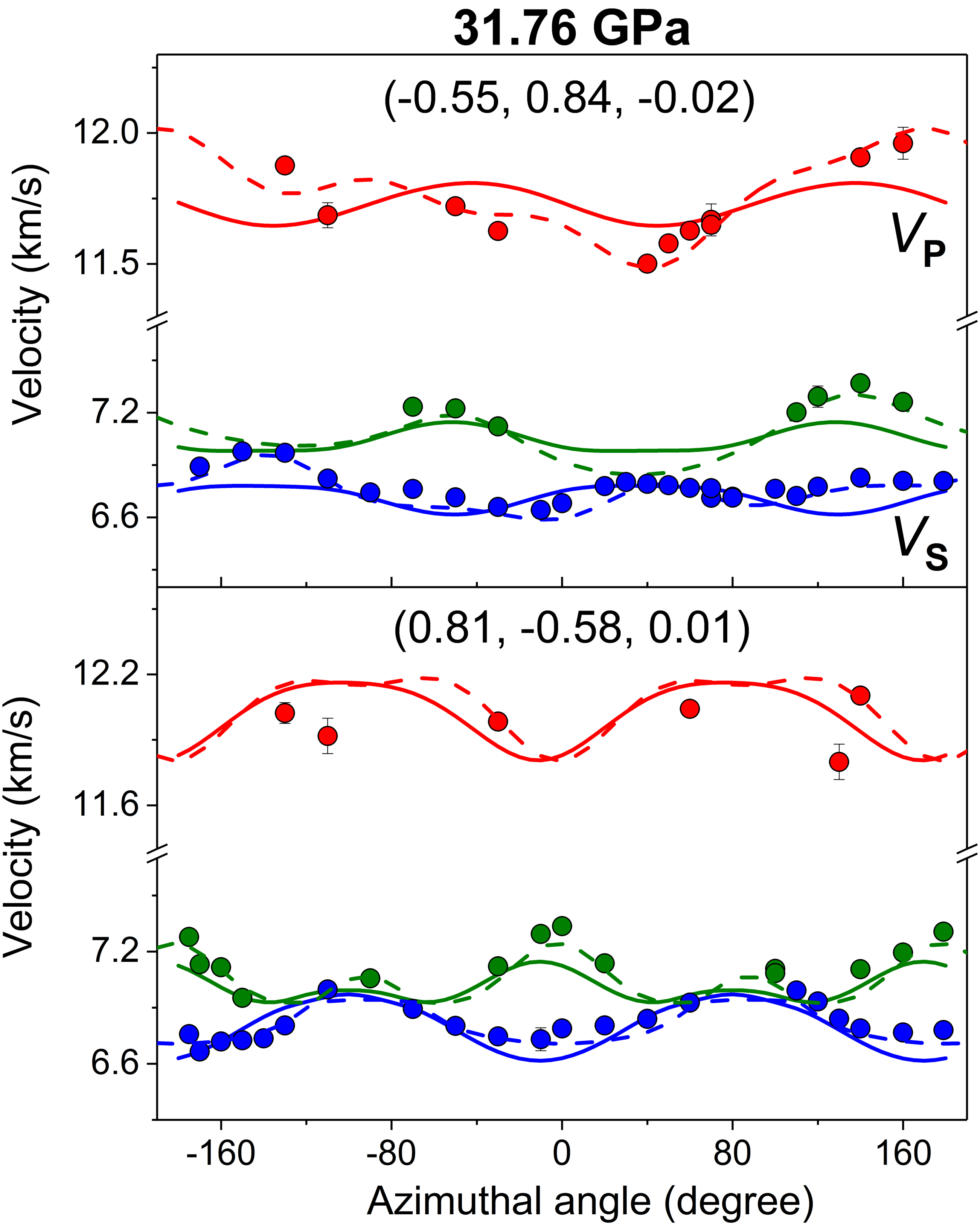

Extended Data Fig. 3 | Modelling the acoustic velocity of bridgmanite to derive C_{ij} at 31.76 GPa. Vertical lines represent standard deviations ($+1\sigma$) and are not shown when smaller than symbols. Solid data points are velocity data from Kurnosov et al.[3]; the dashed lines are velocity-fitting curves from Kurnosov et al.[3]; and the solid lines are velocity-fitting curves using the C_{ij} derived from the covariance matrix analysis in this study. Red, V_P; green, V_s1; blue, V_s2. The orientations of the crystal platelets are given in parentheses.

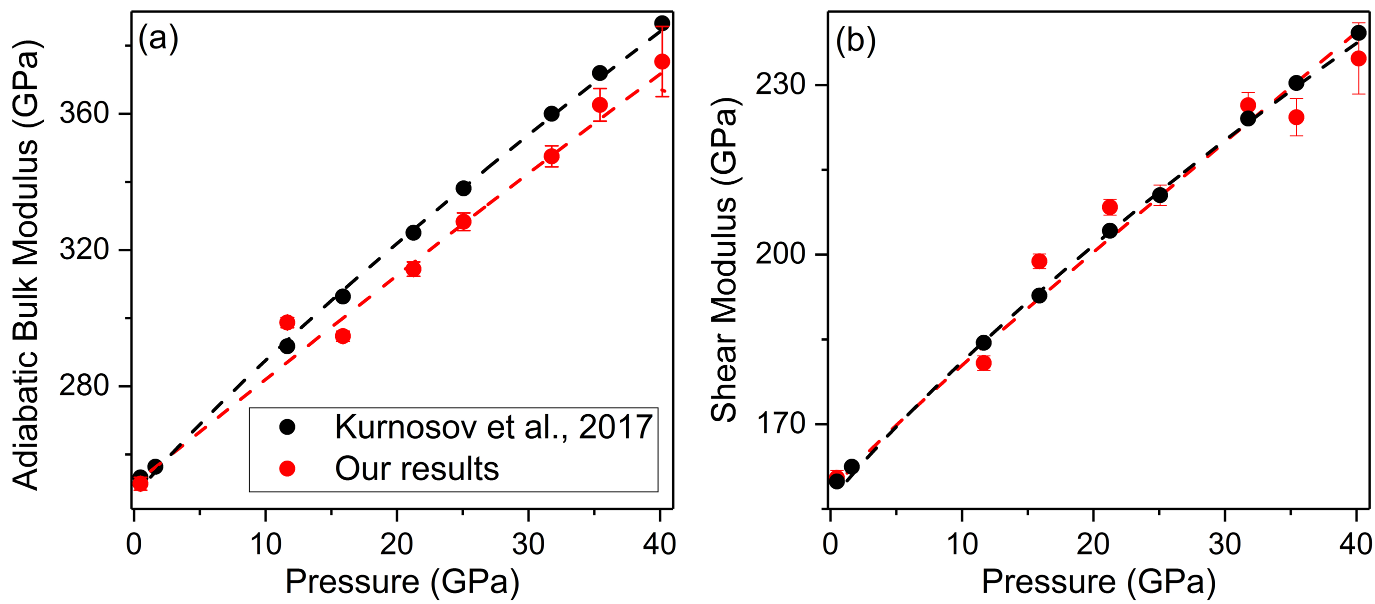

Extended Data Fig. 4 | Adiabatic bulk modulus and shear modulus of bridgmanite ($(Mg_{0.9}Fe_{0.1}Si_{0.9}Al_{0.1})O_3$) at high pressure. a, K_S; **b**, G. Red data points are results using our obtained full elastic constants (C_{ij}); black data points are data reported in Kurnosov et al.[3]. Black and red dashed lines are the best fits to data from Kurnosov et al.[3] and this study, respectively. Error bars represent standard deviations (1σ) and are not shown when smaller than the symbols. In this study, the adiabatic bulk modulus at ambient conditions (K_{S0}) is 250(1) GPa, with the pressure derivative of K_S at 300 K ($K_S{}' = 3.2(2)$), while the shear modulus at ambient conditions (G_0) is 159(1) GPa, with the pressure derivative of G_0 at 300 K ($G' = 2.2(1)$).

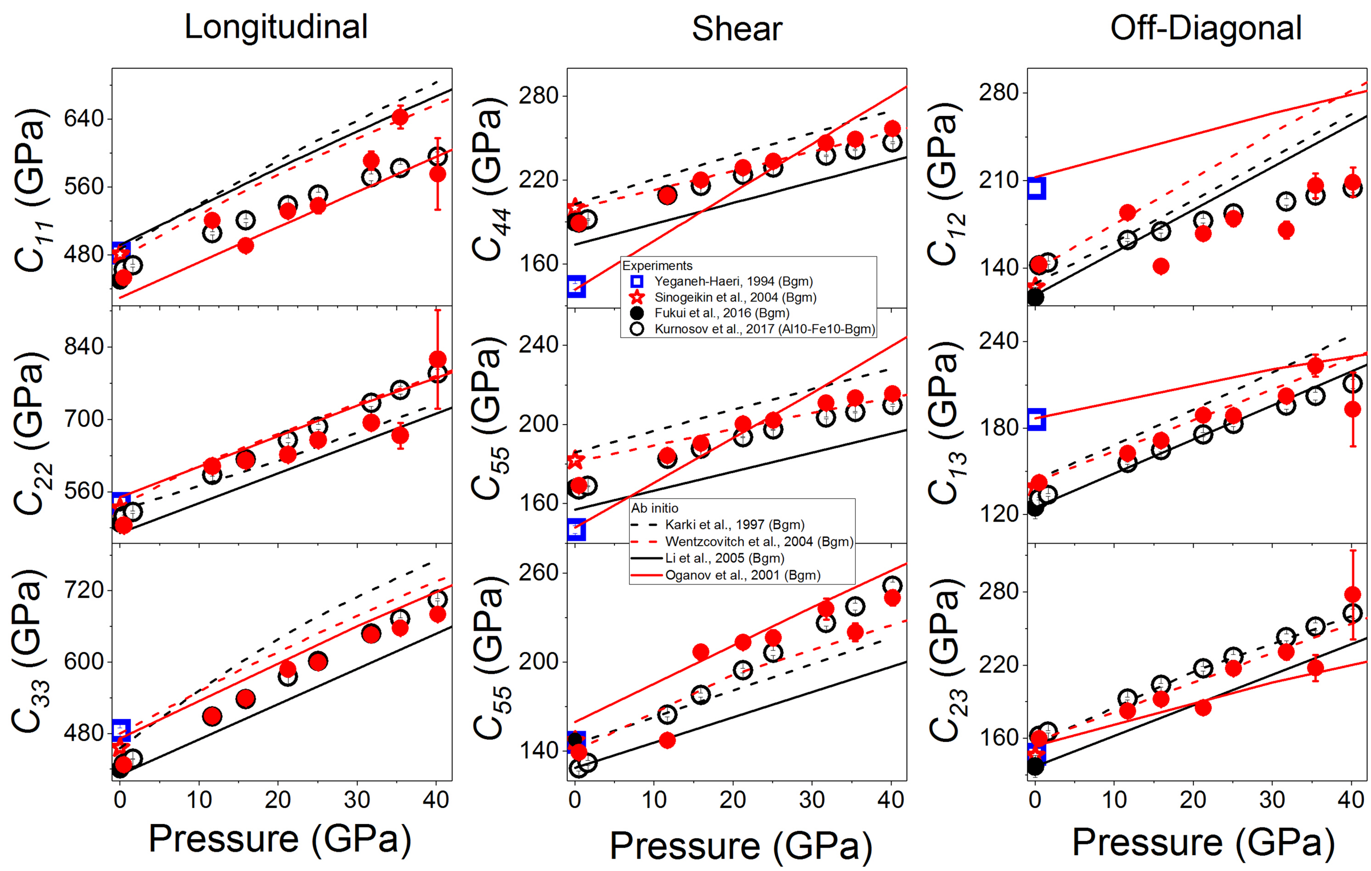

Extended Data Fig. 5 | Comparison of elastic constants of single-crystal bridgmanite as a function of pressure. Bgm, $MgSiO_3$ bridgmanite; Fe10-Al10-Bgm, (Al,Fe)-bearing bridgmanite with a composition of $(Mg_{0.9}Fe_{0.1}Si_{0.9}Al_{0.1})O_3$. Error bars represent standard deviations (1σ) and are not shown when smaller than the symbols. Symbols indicate experimental results from the literature; lines indicate theoretical calculations[3,6,7,16–20]. The filled red circles represent the derived elastic constants in this study using the raw velocity data in Kurnosov et al.[3].

16. Yeganeh-Haeri, A. Synthesis and re-investigation of the elastic properties of single-crystal magnesium silicate perovskite. *Phys. Earth Planet. Inter.* **87**, 111–121 (1994).
17. Fukui, H. et al. Effect of cation substitution on bridgmanite elasticity: a key to interpret seismic anomalies in the lower mantle. *Sci. Rep.* **6**, 33337 (2016).
18. Karki, B. et al. Elastic properties of orthorhombic $MgSiO_3$ perovskite at lower mantle pressures. *Am. Mineral.* **82**, 635–638 (1997).
19. Li, L. et al. Elasticity of (Mg,Fe)(Si,Al)O_3-perovskite at high pressure. *Earth Planet. Sci. Lett.* **240**, 529–536 (2005).
20. Oganov, A. R., Brodholt, J. P. & Price, G. D. Ab initio elasticity and thermal equation of state of $MgSiO_3$ perovskite. *Earth Planet. Sci. Lett.* **184**, 555–560 (2001).

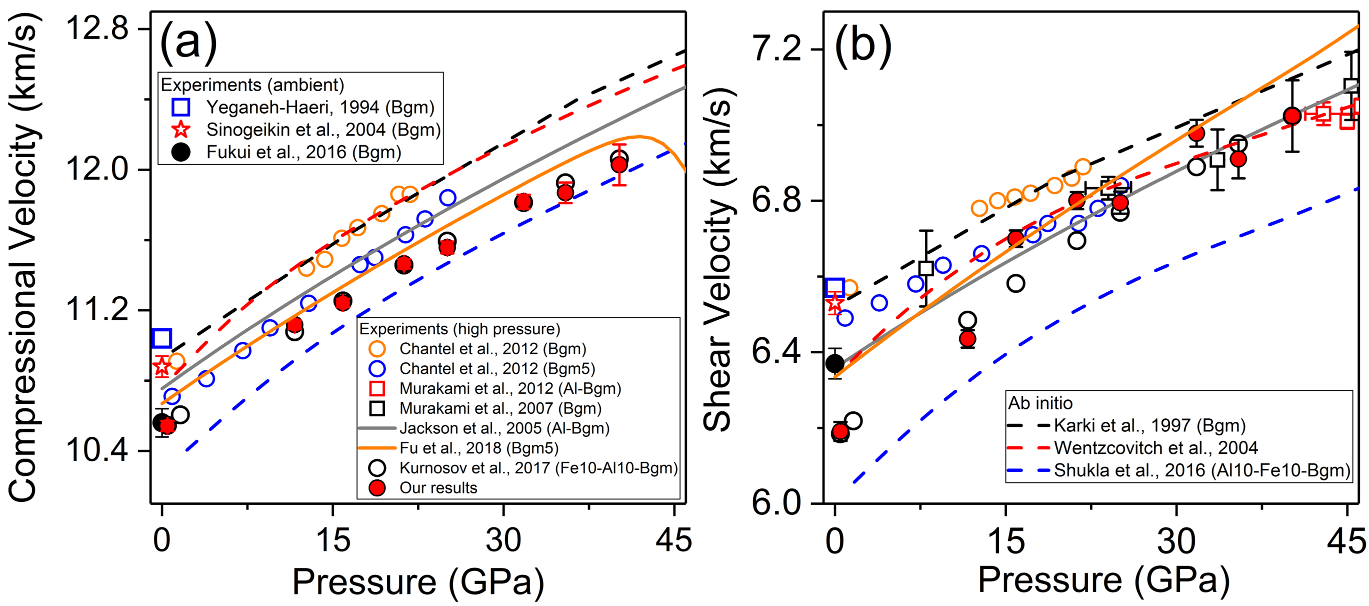

Extended Data Fig. 6 | Comparison of aggregate compressional and shear wave velocities of single-crystal and polycrystalline bridgmanite at high pressure. Symbols and solid lines represent experimental results from the literature; dashed lines indicate theoretical calculations[3,6–11,16–18,21,22]. The solid red circles are the calculated velocities of (Al,Fe)-bearing bridgmanite using the elastic constants derived in this study (Extended Data Fig. 5), while open black circles are from Kurnosov et al.[3]. Error bars represent standard deviations (1σ) and are not shown when smaller than the symbols.

21. Chantel, J., Frost, D. J., McCammon, C. A., Jing, Z. C. & Wang, Y. B. Acoustic velocities of pure and iron-bearing magnesium silicate perovskite measured to 25 GPa and 1200 K. *Geophys. Res. Lett.* **39**, L19307 (2012).

22. Shukla, G., Cococcioni, M. & Wentzcovitch, R. M. Thermoelasticity of Fe^{3+}- and Al-bearing bridgmanite: effects of iron spin crossover. *Geophys. Res. Lett.* **43**, 5661–5670 (2016).

Kurnosov et al. reply

REPLYING TO J.-F. Lin, Z. Mao, J. Yang & S. Fu *Nature* **564**, https://doi.org/10.1038/s41586-018-0741-7 (2018)

In our Letter[1], we reported elastic properties for single crystals of Earth's most abundant mineral, (Al,Fe)-bearing bridgmanite, at pressures of the lower mantle, measured by simultaneous Brillouin spectroscopy and X-ray diffraction. We used our data together with previously published results to model seismic wave velocities for Earth's lower mantle. Contradicting previous work[2], we showed that seismic wave velocities derived for a pyrolitic mantle containing (Al,Fe)-bearing bridgmanite are consistent with the seismic record in the lower mantle up to a depth of about 1,200 km. In the accompanying Comment, Lin et al.[3] claim that our measurements are problematic because we measured insufficient velocity data and used insensitive crystal orientations to constrain the full elastic tensor and hence conclude that the uncertainties given in ref. [1] are underestimated. Here, we address their concerns[3] and show them to be unwarranted.

In our Letter[1], we used a novel experimental approach to reduce uncertainties in the derived elastic constants, which consists of: (a) measurement of two focused-ion-beam-prepared crystals[4,5] of bridgmanite with different crystallographic orientations loaded in a single diamond anvil cell; (b) the simultaneous measurement of acoustic wave velocities and X-ray diffraction determination of the density; and (c) the implementation of a routine to fit the obtained data simultaneously by combining the Christoffel equation with the well established finite strain formalism, which we refer to as a 'global fit'.

In particular, Lin et al.[3] independently analysed our experimental data and obtained uncertainties that are different from those derived from our 'global fit'. Lin et al.[3] employed a standard approach to extract elastic constants from the raw velocity data that we shared with them; that is, velocities measured at a single pressure have been fitted to the Christoffel equation[6]. The uncertainties that Lin et al.[3] report are therefore based on their fit to a single pressure point as opposed to the entire dataset.

In our Letter[1], we measured single-crystal X-ray diffraction of the crystal platelets at each pressure and therefore we know the unit cell volume and the exact crystallographic orientations of both crystals at each pressure. Since the elastic constants at different pressures are not independent but are functions of strain[7], which was derived in our study from experimentally in situ measured unit cell volumes at every pressure, we implemented a routine to fit all the data simultaneously by combining the Christoffel equation with a finite strain formalism (equation (31) in ref. [7]), as stated in our Letter[1]. In this 'global fit', we simultaneously account for: (a) all measured acoustic wave velocities at all pressures; (b) the X-ray orientations measured for each crystal at each pressure; and (c) the measured unit cell volumes at each pressure.

In other words, rather than fitting all elastic constants independently at each pressure, we fit the parameters of the finite strain equation—which describes the change in the elastic constants with pressure—to all data points at all pressures simultaneously. The 'global fit' greatly decreases the number of fitting parameters if enough pressure points are available. In the standard routine, nine independent elastic constants are refined by the data measured at one pressure point, leading to a ratio between observables and refined parameters of about 10 for each individual pressure. In the 'global fit' only nine zero-pressure elastic constants and pressure derivatives (so 18 parameters in total) need to be refined for the entire dataset and these are constrained by all measurements at all nine pressures. In our Letter[1], approximately 1,000 individual velocities were measured in total and the ratio of observables to refined parameters therefore increases to about 50. As a result, the 'global fit' substantially reduces the uncertainties in the derived elastic constants, as shown in refs [1,8].

As pointed out by Lin et al.[3], the chosen crystallographic orientations have different sensitivities to the different elastic constants. In our Letter[1], the reduced sensitivities of certain constants are taken into account and are reflected in larger uncertainties in the respective values. In all our analyses, cross-correlations between the elastic constants are accounted for by an error propagation and correlation analysis performed as part of the 'Origin 2015 (academic)' fitting routine. The reported error in elastic constants is based on the uncertainties in measured velocities and a propagation of fitting uncertainties and correlations of all fitted parameters. It therefore provides a robust measure of uncertainties that captures the limits imposed by the chosen crystallographic directions, limited velocity coverage at high pressures as well as correlation effects (represented by a covariance matrix, as discussed by Lin et al.[3]). As stated in our Letter[1], we also analysed our experimental data using the standard approach and find the results to be consistent with the 'global fit', but with substantially larger uncertainties (Fig. 1). Both fits reproduce the measured velocity curves well (Extended Data Fig. 1).

To quantitatively show the effect of employing the 'global fit' on parameter uncertainties, we carried out a series of robustness tests. We used the elastic constants reported in our Letter[1] to generate a synthetic dataset of velocity distribution for the two crystal platelets used in our experiments. Velocities along random crystallographic orientations were then removed to simulate a lack of coverage caused by peak overlapping with the diamond at high pressure or inefficient elasto-optic coupling. Following this procedure, six datasets with limited data coverage were generated that contain between 4 and 36 measured phonon directions; see also Extended Data Fig. 2. These synthetic datasets

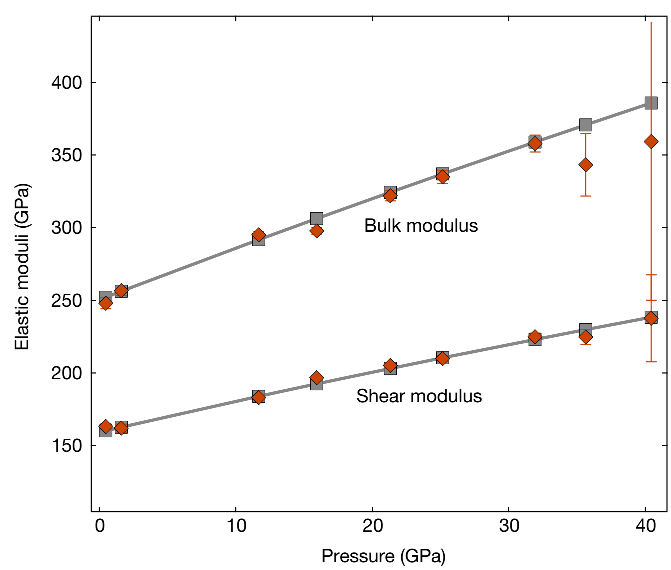

Fig. 1 | Bulk and shear moduli obtained using the 'global fit' (grey squares, solid curves) in comparison to the results of fitting every pressure point individually (red diamonds). Error bars correspond to 2σ. Both methods agree within uncertainties.

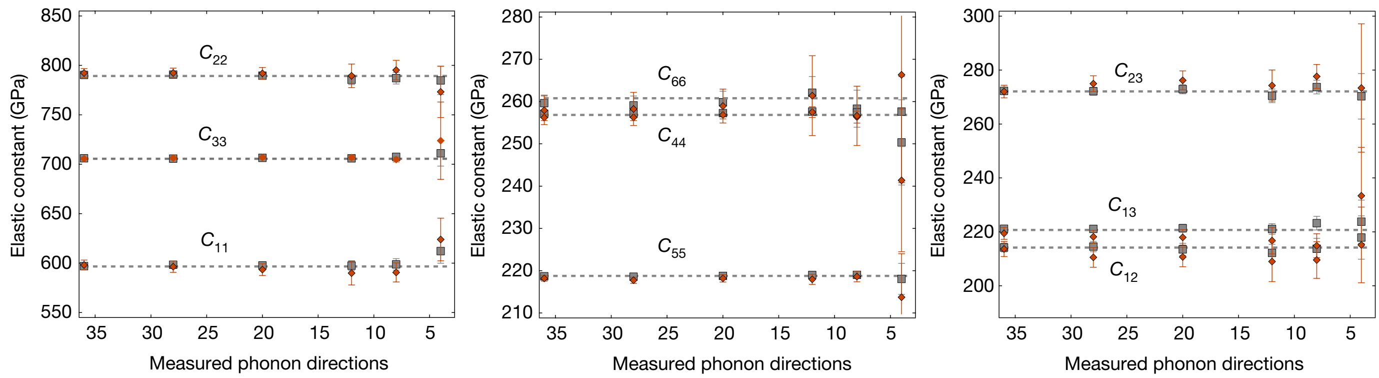

Fig. 2 | Elastic constants derived at 40.4 GPa by fitting the synthetic data. Grey squares are the results of the 'global fit'; red diamonds are the results of individual fits. Error bars refer to 1σ. The individual fits show systematically larger errors and start to deviate from the real values (dotted lines) when data coverage is limited. The results of the 'global fit' stay close to the real values even when few phonon directions are measured. We note that in the experiments reported in our Letter[1], we measured about 15 (for compressional velocities V_P) to 30 (for shear-wave velocities V_S) phonon directions at the highest pressure despite overlap with the diamond shear peak, that is, our dataset contains substantially more points than many of those tested here.

were then analysed in three ways: (a) using the standard approach, where all elastic constants and the orientation of the crystal planes are refined for every pressure individually, as has been done in previous Brillouin studies, for example, refs [9–11]; (b) as above, but fixing the orientation of the crystal planes to the values measured by X-ray diffraction, referred to as an 'individual fit' here; (c) using the 'global fit', where all synthetic velocity data and X-ray volumes are simultaneously inverted to derive the zero-pressure elastic constants and their pressure derivatives.

We found that the standard approach produces the same results and similar uncertainties as the other two routines if data coverage is very good. It fails, however, to refine the elastic constants when fewer velocities are measured (the threshold in our test was about 20 phonon directions). Once the orientations of the crystal planes are known, however, from in situ X-ray diffraction, fewer velocity measurements are required to constrain all elastic constants (Fig. 2, red diamonds). Finally, the application of the 'global fit' leads to a significant reduction in uncertainties and reproduces almost all the initial elastic constants at the highest experimental pressure within 1σ, where σ is the standard error on the respective fitting parameter as given by the fitting procedure in the program 'Origin' (grey squares in Fig. 2). Figure 3 shows the deviation of all 'global fit' elastic constants from the values used to generate our synthetic dataset ('real' values) against their respective 'global fit' fitting uncertainties. The deviation of almost all (or all) elastic constants from the real value is smaller than the reported 1σ (or 2σ).

Our tests using the synthetic data show both that the global fit allows the elastic constants to be well constrained even when some gaps in velocity data appear at the highest pressures and that reported fitting uncertainties are accurate. We thus feel that the concerns raised by Lin et al.[3] are unwarranted.

Lin et al.[3] conclude their Comment by stating that the uncertainties in our data preclude any inference about (a) the existence of metallic iron in the lower mantle or (b) a possible change of ferric iron content with depth in bridgmanite. Although we entirely agree with assertion (a) and have never argued for the possibility of resolving the presence of metallic iron directly from our modelled velocity data (see also figure 3 in ref. [1]), we feel that a discussion about assertion (b) is warranted. There is a subtle, but systematic, deviation in modelled wave velocities from PREM, which is difficult to explain even when uncertainties increase at higher temperatures. In our Letter[1], we discuss the possibility that this deviation reduces if the bridgmanite ferric iron content decreases with depth. Given the importance of such a scenario for our understanding of deep-mantle geophysics and geochemistry, we strongly feel that this finding warrants a discussion and will guide future research. In fact, a recent publication using a complementary approach has independently reported evidence for a decrease in the ferric iron content of the lower mantle with depth[12].

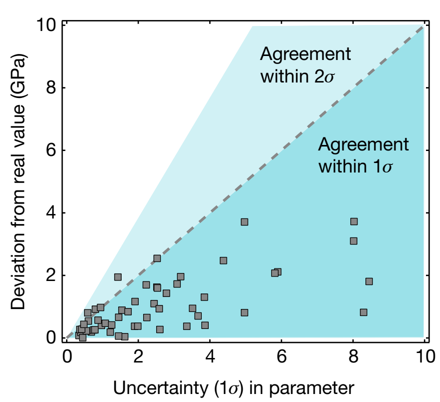

Fig. 3 | Uncertainty analysis for the 'global fit'. Deviation of all 'global fit' elastic constants at 40.4 GPa (that is, all constants derived from all six models) from the values used to generate the dataset (the 'real' values) as a function of the fitting uncertainties calculated by the least-squares routine. Almost all derived constants agree with the real values within 1σ (shown as the dark-blue region, that is, all data below the dotted grey line); all constants agree within 2σ (shown as the light-blue region).

Data availability

The datasets generated and analysed during this study and the Origin routine that we used are available from the corresponding author on reasonable request.

A. Kurnosov[1], H. Marquardt[1,2]*, D. J. Frost[1], T. Boffa Ballaran[1] & L. Ziberna[1]

[1]Bayerisches Geoinstitut BGI, University of Bayreuth, Bayreuth, Germany.
[2]Department of Earth Sciences, University of Oxford, Oxford, UK.
*e-mail: Hauke.Marquardt@uni-bayreuth.de19 December 2018

1. Kurnosov, A., Marquardt, H., Frost, D. J., Boffa Ballaran, T. & Ziberna, L. Evidence for a Fe^{3+}-rich pyrolitic lower mantle from (Al,Fe)-bearing bridgmanite elasticity data. *Nature* **543**, 543–546 (2017); Author Correction *Nature* **558**, E3 (2018).
2. Murakami, M., Ohishi, Y., Hirao, N. & Hirose, K. A perovskitic lower mantle inferred from high-pressure, high-temperature sound velocity data. *Nature* **485**, 90–94 (2012).
3. Lin, J.-F, Mao, Z., Yang, J. & Fu, S. Elasticity of lower-mantle bridgmanite. *Nature* **564**, https://doi.org/10.1038/s41586-018-0741-7 (2018).

4. Marquardt, H. & Marquardt, K. Focused ion beam preparation and characterization of single-crystal samples for high-pressure experiments in the diamond-anvil cell. *Am. Mineral*. **97**, 299–304 (2012).
5. Schulze, K., Buchen, J., Marquardt, K. & Marquardt, H. Multi-sample loading technique for comparative physical property measurements in the diamond-anvil cell. *High Press. Res*. **37**, 159–169 (2017).
6. Speziale, S., Marquardt, H. & Duffy, T. S. Brillouin scattering and its application in geosciences. *Rev. Miner. Geochem*. **78**, 543–603 (2014).
7. Stixrude, L. & Lithgow-Bertelloni, C. Thermodynamics of mantle minerals—I. Physical properties. *Geophys. J. Int*. **162**, 610–632 (2005).
8. Buchen, J. et al. High-pressure single-crystal elasticity of wadsleyite and the seismic signature of water in the shallow transition zone. *Earth Planet. Sci. Lett*. **498**, 77–87 (2018).
9. Speziale, S. & Duffy, T. S. Single-crystal elasticity of fayalite to 12 GPa. *J. Geophys. Res*. **109**, B12202 (2004).
10. Speziale, S. & Duffy, T. S. Single-crystal elastic constants of fluorite (CaF_2) to 9.3 GPa. *Phys. Chem. Miner*. **29**, 465–472 (2002).
11. Marquardt, H., Speziale, S., Reichmann, H. J., Frost, D. J. & Schilling, F. R. Single-crystal elasticity of $(Mg_{0.9}Fe_{0.1})O$ to 81 GPa. *Earth Planet. Sci. Lett*. **287**, 345–352 (2009).
12. Shim, S.-H. et al. Stability of ferrous-iron-rich bridgmanite under reducing midmantle conditions. *Proc. Natl Acad. Sci. USA* **114**, 6468–6473 (2017).
13. Sinogeikin, S. V. & Bass, J. D. Single-crystal elasticity of pyrope and MgO to 20 GPa by Brillouin scattering in the diamond cell. *Phys. Earth Planet. Inter*. **120**, 43–62 (2000).

Author contributions A.K., H.M., D.J.F. and T.B.B. discussed the content. A.K. performed the robustness test. H.M. wrote the paper draft. All authors commented on the manuscript.

Competing interests Declared none.

Additional information
Extended data accompanies this Reply.
Supplementary information accompanies this Reply.
Reprints and permissions information is available at https://www.nature.com/reprints.
Correspondence and requests for materials should be addressed to H.M.

https://doi.org/10.1038/s41586-018-0742-6

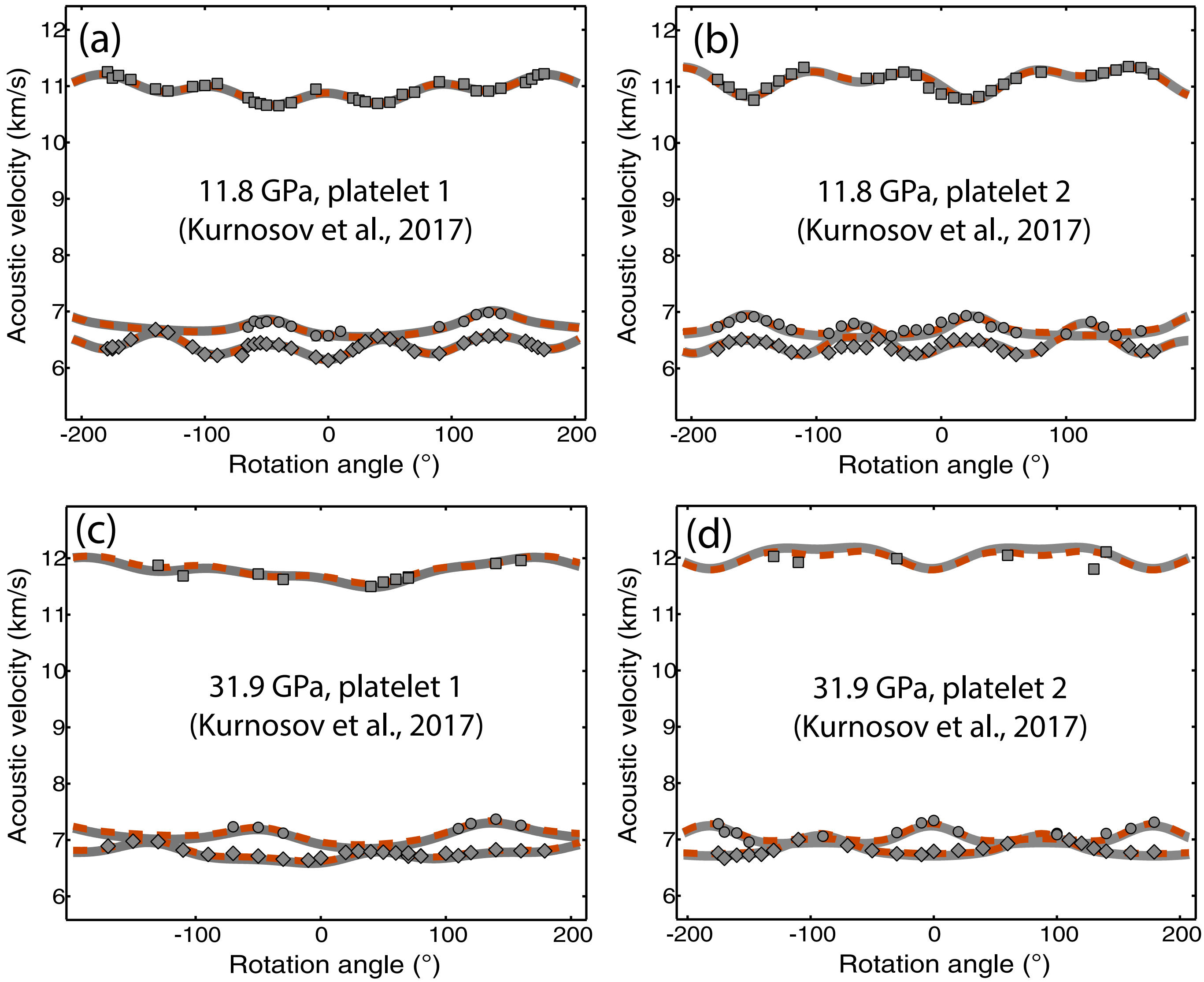

Extended Data Fig. 1 | Raw data collected on single-crystal bridgmanite at two selected pressures and fits from our Letter. The solid curves are fits to the grey data using the best-fit global model (the 'global fit' of ref. [1]) and the red dashed curves are individual fits. **a**, **c**, Platelet 1. **b**, **d**, Platelet 2. **a**, **b**, Data collected at 11.8 GPa; **c**, **d**, data collected at 31.9 GPa. We note that the orientation of the crystals changed slightly during pressure increase, but was measured at every pressure in our experiment. A 'tilt' correction was employed for crystal platelet 1, as mentioned in our Letter[1]. The procedure is further explained in the Supplementary Information (containing the raw data).

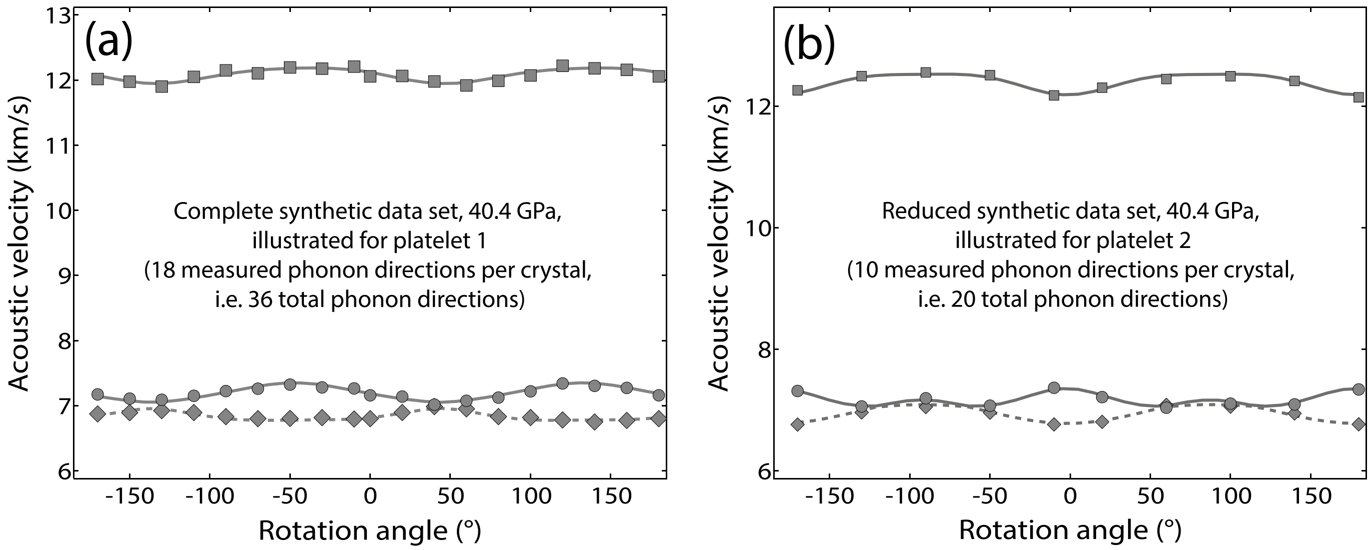

Extended Data Fig. 2 | Illustration of how the synthetic dataset at 40.4 GPa was generated using the elastic constants reported in our Letter. For every pressure point and platelet, velocities in 18 propagation directions were calculated over an angular range of 360° to simulate in-plane rotations between individual measurements that are representative of our low pressure measurements where no overlap of peaks occurred (solid symbols). We randomly changed the velocity values by up to 0.5% to simulate errors typical for single velocity measurements by Brillouin spectroscopy in the diamond anvil cell[13]. **a**, Illustration of a complete velocity dataset, using crystal platelet 1 as an example. **b**, Illustration of a reduced dataset, using crystal platelet 2 as an example. This assumes limited data availability owing to peak overlap or elasto-optic coupling. The example in **b** corresponds to a situation where 20 directions have been measured in total (10 on each crystal). Solid and dotted curves are results from the 'global fit'.